RSC Advances

ROYAL SOCIETY OF CHEMISTRY

www.rsc.org/advances

High cobalt oxide concentrations were able to shield the microporous silica network from excessive structural rearrangement during harsh hydrothermal testing

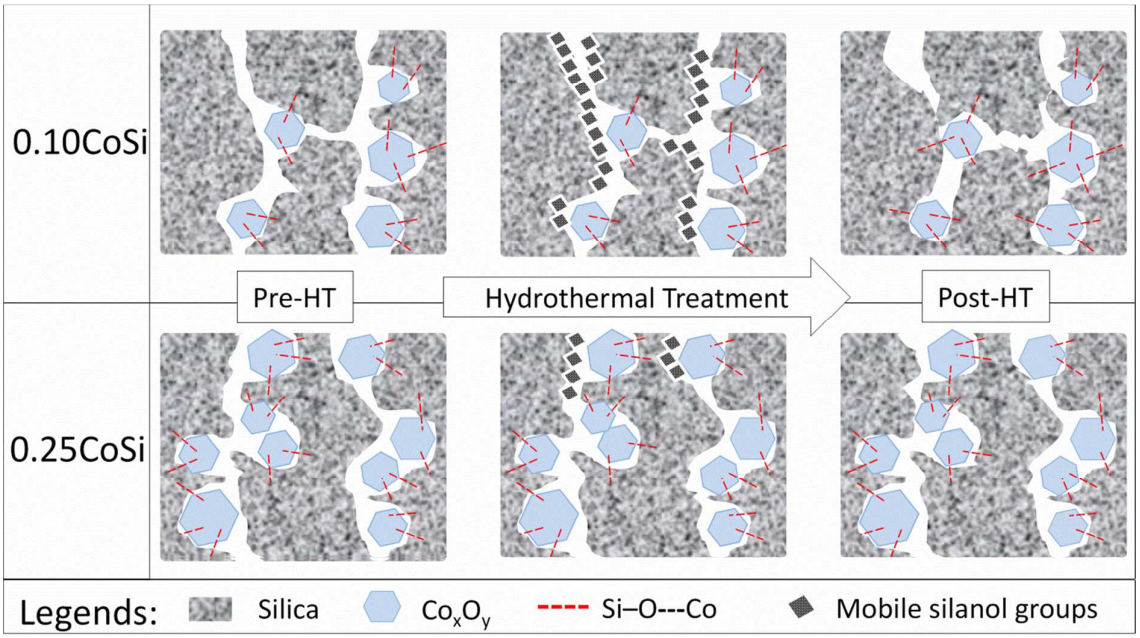

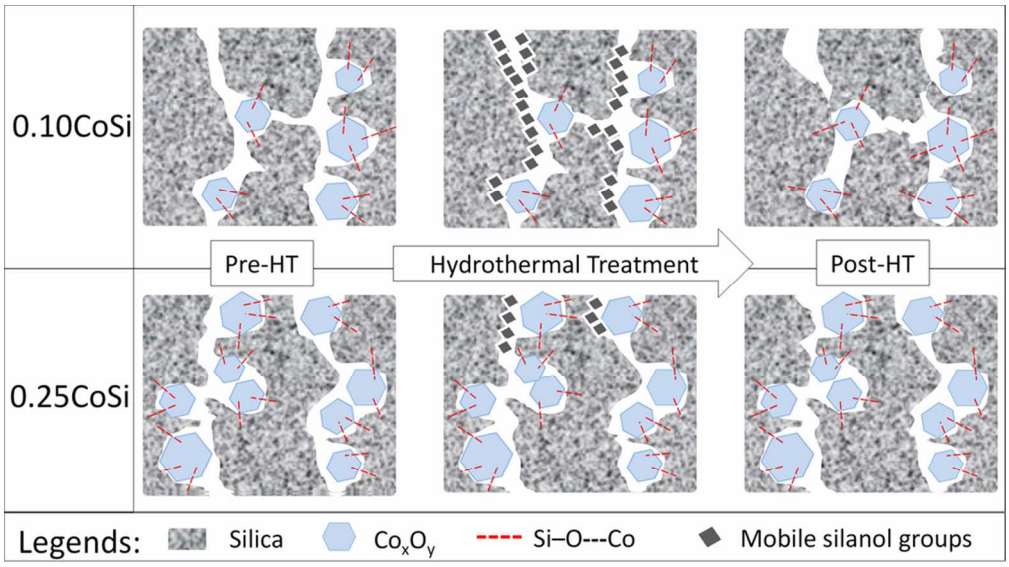

High cobalt oxide concentrations were able to shield the microporous silica network from excessive structural rearrangement during harsh hydrothermal testing
89x49mm (300 x 300 DPI)

Physicochemical characterization and hydrothermal stability investigation of cobalt-incorporated silica xerogels

[ab]Liang Liu, [a]David K. Wang, [ab]Dana. L. Martens, [ab]Simon Smart*, [c]Ekaterina Strounina, [ab]João C. Diniz da Costa

[a] The University of Queensland, FIMLab – Films and Inorganic Membrane Laboratory, School of Chemical Engineering, Brisbane, QLD 4072, Australia

[b] Cooperative Research Centre for Greenhouse Gas Technologies (CO2CRC)

[c] Centre for Advanced Imaging, The University of Queensland, Brisbane QLD 4072, Australia

*Corresponding author. Tel.: +61 7 3365 8591; Fax: +61 7 3365 4199

Email: *s.smart@uq.edu.au*

Highlights:

- Hydrothermal stable microporous cobalt silica xerogels were successfully prepared demonstrating less than 25 % surface area loss after exposing to a harsh condition of 75 mol% vapour at 550 °C for 40 h.
- The hydrothermal stability of the xerogels was highly dependent of the cobalt concentration.
- High concentration of cobalt oxides can shield the silica network from further condensation reaction, conferring improved hydrothermal stability.

Abstract

The hydrothermal stability of the cobalt oxide silica xerogels was comprehensively investigated, including the effect of Co/Si molar ratio (0.00–0.50), vapour content (0–75 mol%), exposure time (0–100 h) and temperature (250–550 °C). Physicochemical properties of the xerogels were characterized by nitrogen sorption, FTIR, solid-state ^{29}Si NMR (CP/MAS), micro-Raman, XRD and HR-TEM techniques. The structural characterization indicated that increasing cobalt incorporation inhibited the degree of condensation in the silica network, and that the formation of tricobalt tetroxide (Co_3O_4) nanocrystals in the silica matrix was only observed in high cobalt loading samples (Co/Si ≥ 0.25). The hydrothermal stability of the xerogels assessed by N_2 sorption was found to be strongly dependent on the cobalt loading; particularly when the presence of Co_3O_4 in the silica matrices was implicated. For the unstable xerogels (Co/Si < 0.25), the material's stability was significantly decreased by both vapour content and exposure time, resulting in an almost 90 % surface area reduction. On the other hand, the high cobalt loading xerogels (Co/Si ≥ 0.25) were found to contain Co_3O_4 and were much more stable, losing less than 25 % of surface area and maintaining microporous structure after exposing to a harsh condition of 75 mol% vapour at 550 °C for 40 h. A structural model is proposed whereby the cobalt oxide particles 'shield' the silica matrix and inhibit the hydrolysis and condensation of the silica in the pores walls. This effectively limits the structural rearrangement that hydrothermal treatment typically invokes and therefore confers improved hydrothermal stability.

Keywords: silica xerogels, hydrothermal stability, tricobalt tetroxide (Co_3O_4)

1. Introduction

The silica sol-gel process represents a powerful, yet simple approach to synthesise functional materials for membranes, catalysts, sensors and optical applications.[1-5] This process is versatile, with the ability to tailor structures with controllable pore sizes, particularly around 3 to 5 Å for molecular gas sieving separations.[6-8] In this process, the condensation reaction of silica alkoxides is inhibited, thus generating uncondensed species known as silanols (Si–OH). Silanol moieties freely interpenetrate one another as they are forced into close proximity[9] during the sol-gel process leading to gelation and silica film formation.

From one perspective, this process is ideal as the interpenetration of silanol groups in the silica matrix provides an ideal synthesis environment for molecular pore size tailoring. On the other hand, silanol groups are hydrophilic, and silica matrices undergo structural rearrangement in the presence of water,[10] particularly within the first day of exposure.[11] As a consequence, the pore sizes enlarge, leading to ineffectual gas separation and loss in membrane performance.[12, 13]

To address the hydro instability of porous silica matrices, several groups have embedded structural stabilising entities into the silica matrix. These have included covalently bonded templates,[14, 15] carbonisation of cationic surfactants[16] and doping of metal oxides based on nickel,[17] cobalt[18, 19] and niobia.[20] The incorporation of metal oxides such as cobalt may prevent thermally-induced movement of silanol groups resulting in rearrangement of the silica network under hydrothermal conditions,[18] thus rendering silica membranes hydrostable. Nevertheless, many of the hydrothermal investigations involving silica membrane materials reported in the literature were carried out under conditions of moderate temperatures and generally at low steam concentrations. This is a significant limitation regarding the current body of literature, as there is no proof that porous silica structures can withstand long term exposures at high steam concentration and temperatures. Of the limited work performed in this area, the most significant studies showed that cobalt oxide silica membranes operating at high temperatures (500 °C) gradually decline in performance.[18, 21] Interestingly Battersby and co-workers[22] showed that the densification of the silica matrix occurred for both cobalt oxide silica and pure silica matrices, though the former maintained microporosity after high pressure exposure in an autoclave, contrary to the meso-macroporisity for the pure silica. Hence, the incorporation of metal oxide into silica matrices has been shown to improve

hydrothermal stability. Despite these studies, there is a paucity of comprehensive hydrothermal investigations to fully understand how these properties may be conferred.

This work systematically investigated the stability of cobalt oxide incorporated silica xerogel matrices under various hydrothermal treatment conditions, including harsh conditions of high temperature and high water content, to provide further knowledge in the structure-property-performance relationship. Sol-gel processing was used to synthesize cobalt oxide silica xerogels containing a parametric increase of Co/Si molar ratio from 0.00 (blank sample – pure silica) to 0.50. The resultant xerogels were tested under different hydrothermal conditions as a function of water vapour concentration (10–75 mol%), exposure time (20–100 h) and temperatures (250–550 °C). Finally, the physicochemical properties of xerogel matrices were characterized by nitrogen physisorption, ATR-FTIR, solid state ^{29}Si CP/MAS NMR, micro-Raman, XRD and HR-TEM techniques.

2. Experimental

Cobalt silica sols with a Co/Si molar ratio ranging between 0.00 and 0.50 were prepared by a sol-gel method described elsewhere.[21] Briefly, cobalt nitrate hexahydrate ($Co(NO_3)_2 \cdot 6H_2O$, 98 %, Sigma-Aldrich) was dissolved in a solution of hydrogen peroxide (H_2O_2, 30 wt%) and ethanol (EtOH, 99 %, AR grade). The mixture then was cooled down to 0 °C using an ice bath. Tetraethoxysilane (TEOS, 99 %, Fluka) was added drop-wise and stirred for 3 h to achieve a final molar ratio of 255: 80: 4: 0–2: 9 for the EtOH: H_2O: TEOS: $Co(NO_3)_2 \cdot 6H_2O$: H_2O_2 sol. The pH was measured between ~3.5 and 4 which is above the isoelectric point of the silica particles (pH 1~3).[23] All the sols remained clear and transparent during the sol synthesis which indicated that the sols were stable and homogenous. The sol was dried in an oven at 60 °C for 96 h. The dried xerogels were ground into a fine powder and calcined in an air atmosphere in a temperature-controlled furnace at 630 °C for a hold time of 2.5 h with heating/cooling rates of 1 °C min^{-1}. The 'as-synthesized' materials are hereafter denoted by XCoSi, where X is the molar ratio of cobalt to silicon, e.g. 0.10CoSi for the cobalt oxide silica xerogel with 0.10 Co/Si, and 0.00CoSi for pure silica.

Nitrogen sorption experiments were carried out on a Micromeritics TriStar 3020 analyzer after degassing under vacuum on a Micromeritics VacPrep061 at 200 °C for a minimum of 6 h. The specific surface areas were calculated from the adsorption isotherms via a multi-point Brunauer-Emmett-Teller (BET) model. The pore volume was obtained from the amount adsorbed at a relative pressure (P/P_o) of 0.95. Fourier transform infra-red (FTIR) spectra were

collected with a Shimadzu IRAffinity-1 with a Pike MIRacle diamond attenuated total reflectance (ATR) attachment. Spectra were taken over a wavenumber range of 4000–500 cm^{-1}. Peak fitting of the FTIR spectra was performed using the Fityk software (version 0.9.4). The peak position and peak height were allowed to vary between samples to achieve the best possible fit.

Cross-polarization magic-angle-spining (CP/MAS) solid-state ^{29}Si nuclear magnetic resonance spectroscopy (NMR) was performed on an Avance III spectrometer (Bruker), operating at 300.13 MHz for ^{1}H and 59.627 MHz for ^{29}Si. The samples were placed in a 4 mm zirconium rotor and rotated at magic angle with 7 kHz frequency. The spectra were recorded using the SP-hpdec technique (single pulse with high power proton decoupling). The parameters included 42 ms acquisition time with sweep width of 30 kHz; 2K data points were collected. Cross-polarisation time was 5 ms. High-power decoupling at 73.53 kHz was applied using tppm15 scheme. Between 200 and 1000 scans were collected. The recycle time was determined as 150 and 500 s, according to the sample's T_1. Peak fitting of the NMR spectra was performed in a similar way as FTIR spectra.

Micro-Raman spectra were acquired using a Nicolet Almega XR dispersive Raman spectrometer coupled to an Olympus microscope using a He: Ne laser (633 nm) over 2000–70 cm^{-1}. X-ray diffraction (XRD) was conducted on a Bruker D8 Advance fitted with graphite monochromators using Cu-Kα radiation at an operating voltage of 40 kV and amperage of 40 mA. Full scans were collected over 20–80 °2θ with a scanning rate of 3.2 s/step, with focused scans collected between 32–43 °2θ with a scanning rate of 30 s/step.

High-resolution transmission electron microscopy (HR-TEM) was performed on a JEOL2100 equipped with an energy-dispersive X-ray spectroscopy (EDS) accessory. TEM grids were prepared by drop-casting an aliquot of xerogel ethanol suspension onto a holey carbon film and air-dried before examination.

Hydrothermal treatment (HT) of the as-synthesized xerogels (0.00-0.50 Co/Si) was conducted in a customized rig (see Fig. 1). The temperature of the furnace was controlled by a PID temperature controller. The water flow rate was controlled by a Bronkhorst flow controller and was preheated to 200 °C in the vaporizer. The carrier gas flow rate (N_2) was set to 40 ml min^{-1}. The xerogels were placed inside the quartz tube furnace and tested under different hydrothermal conditions (Table 1) to investigate the effect of water vapour content (10–75 mol%; with equivalent water flow rates of 0.2–5.4 g h^{-1}), exposure time (20–100 h)

and temperature (250–550 °C) on the structural surface properties which were evaluated based on the N_2 isotherm profile and surface area.

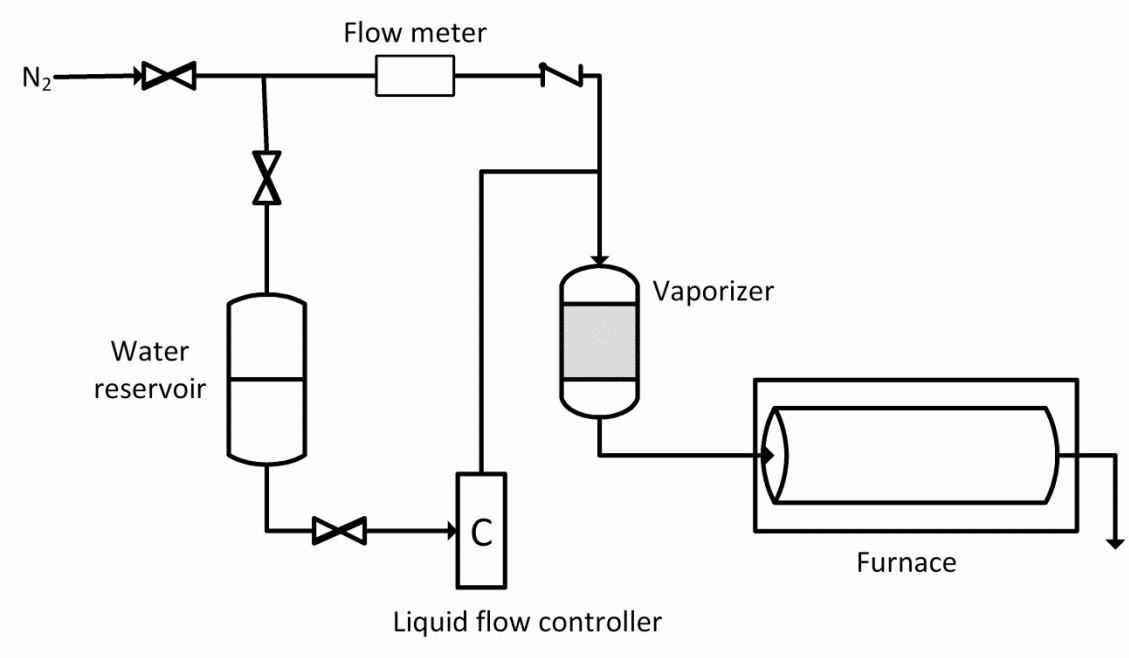

Figure 1: Illustration of customized hydrothermal test rig

Table 1: Hydrothermal test conditions of the as-synthesized cobalt silica xerogels

Samples	Temperature (°C)	Vapour content (mol%)	Time (h)	Water flow rate (g h^{-1})
XCoSi (X=0.00, 0.05, 0.10, 0.15, 0.25 and 0.50 of Co/Si)	550	10	20	0.2
		25		0.6
		50		1.8
		75		5.4
	550	25	20	0.6
			100	
	550	75	20	5.4
			40	
	250	75	20	5.4
	350			
	550			

3. Results and discussion:

3.1 As-synthesized xerogels before hydrothermal treatment

The FTIR spectra of the as-synthesized xerogels are shown in Fig. 2(a). The spectra agree well with previously reported FTIR investigations of silica-based materials.[24, 25] The bands near the wavenumber region of 1220 and 1080 cm^{-1} correspond to the longitudinal optic (LO) and the transversal optic (TO) modes of the asymmetric stretching vibrations of siloxane

groups (Si–O–Si), respectively.[26] In addition, the peak centered at 800 cm^{-1} was assigned to the symmetric stretching vibrations of the same groups.[26] A shoulder peak centered at 950 cm^{-1} can be attributed to the Si–O^- stretching vibration of the Si–OH.[27] Also shown in Fig. 2(a), the peak around 670 cm^{-1} was allocated to the vibrational stretching modes of Co(III)–O bonds in tricobalt tetroxide (Co_3O_4).[28, 29] The formation of Co_3O_4 was clearly influenced by the cobalt loadings. At low Co/Si molar ratio (Co/Si < 0.25), no cobalt species can be detected by FTIR which is in good agreement with reports published elsewhere.[28, 29] The presence of Co_3O_4 can only be observed in the high cobalt loading xerogels; in 0.25CoSi and 0.50CoSi, especially.

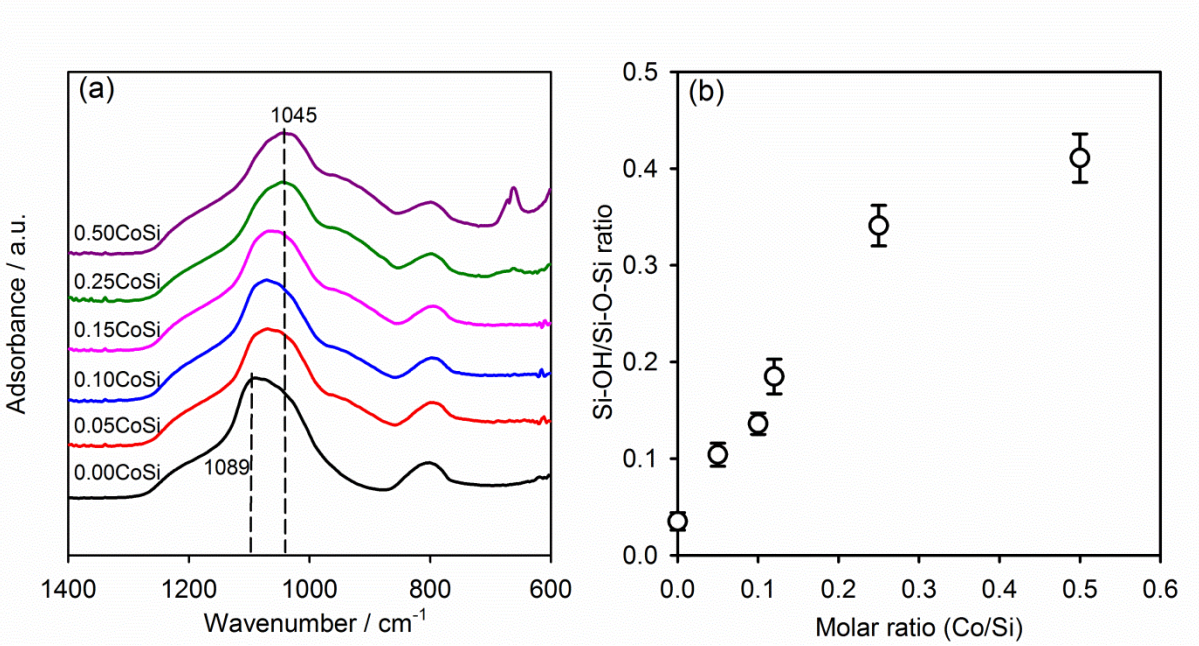

Figure 2: (a) FTIR spectra of the as-synthesized xerogels and (b) Ratio of silanol (950 cm^{-1}) peak area to siloxane (1070 cm^{-1}) peak area as a function of Co/Si molar ratio

One interesting observation in the spectra was the correlation between a systematic redshift of the Si–O–Si TO mode with increasing Co/Si molar ratio. Specifically, the frequency of this vibrational mode shifted from ~1089 cm^{-1} for 0CoSi to ~1045 cm^{-1} for 0.50CoSi possibly due to an increased interaction between the silica and the cobalt oxides.[30] Furthermore, the peak intensity of the silanol band increases as a function of Co/Si molar ratio by visual inspection. Therefore, the bands relating to the silanol (950 cm^{-1}) and siloxane (1070 cm^{-1}) groups were decomposed to estimate and compare the degree of condensation between the xerogel matrices; where a low silanol-to-siloxane ratio correlates to a high

degree of condensation. Fig. 2(b) shows the peak area ratio of silanol peak over the siloxane peak as a function of Co/Si molar ratio. The ratio increases linearly from 0.03 for 0.00CoSi to 0.35 for 0.25CoSi, reaching 0.41 for 0.50CoSi. It is clear that the addition of cobalt into the silica matrix increases the concentration of hydrophilic silanols with respect to the siloxane groups. In another words, the degree of condensation was reduced by the cobalt incorporation.

The degree of condensation of the silica network was further investigated by cross-polarization magic-angle-spining (CP/MAS) solid-state ^{29}Si NMR (Table 2). See Fig. S1 in the Supplementary Information for a peak decomposed NMR spectrum of 0.10CoSi, as an example. In these samples, the typical Q^n (Q^2, Q^3 and Q^4) species of the SiO_4 tetrahedron were all observed and in good agreement with literature values (*n* represents the number of tetrahedral bonding neighbours).[10] The total concentration of Q^2 and Q^3 species (silanols) increased from 11 % for 0.10CoSi to approximately 23 % for 0.50CoSi at the expense of Q^4 groups (siloxanes). These results are consistent with the FTIR findings.

Table 2: ^{29}Si NMR CP/MAS peak centers (ppm) and peak area concentrations (%)

Samples	Q^2		Q^3		Q^4	
	Center	Area	Center	Area	Center	Area
0.10CoSi	-90	5	-99	6	-113	89
0.25CoSi	-91	6	-102	12	-116	82
0.50CoSi	-90	7	-101	16	-115	77

To further probe the chemical structure of the xerogels, Raman spectroscopy was carried out. Fig. 3 shows the Raman spectra of all the xerogel samples. For 0.00CoSi, the bands at ~430 , 800, 1070 and 1180 cm^{-1} were assigned to the Si–O–Si vibrational modes of an amorphous silica network.[27] Ascribed as defects, D1 and D2, the narrow bands at ~490 and ~650 cm^{-1} were attributed to the three- and four-membered ring structure of the silica network, respectively.[31] In all cobalt-incorporated silica xerogels these characteristic Raman bands of silica were masked by a broad emmision centred at around 1200 cm^{-1}. This emission may be attributed to fluorescence caused by cobalt ions coordinated with the silica matrix. In the 0.25CoSi and 0.50CoSi spectra, intense peaks at ~190 cm^{-1} (F_{2g}), 480 cm^{-1} (E_g) and 690 cm^{-1} (A_{1g}) along with peaks of lesser intensition at 520 cm^{-1} (F_{2g}) and 618 cm^{-1} (F_{2g}) were assigned to the vibrational models of Co_3O_4 ,[32, 33] which is consistent with the FTIR results.

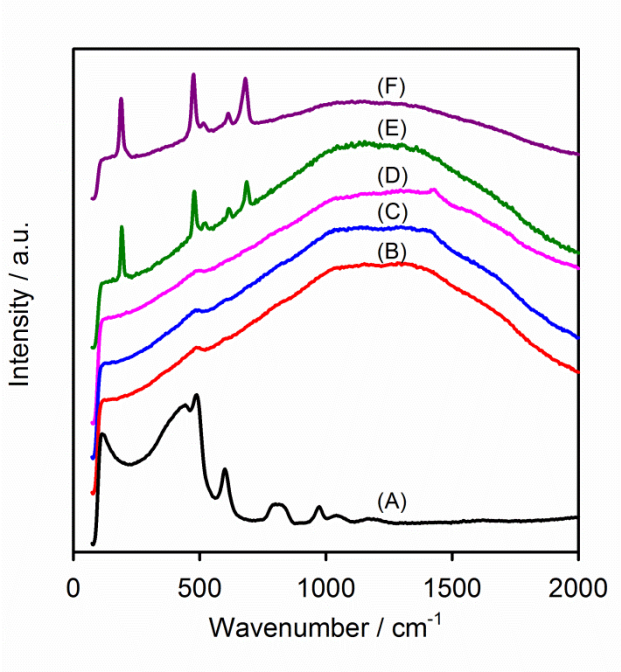

Figure 3: Raman spectra of the as-synthesized xerogels: (A) 0.00CoSi, (B) 0.05CoSi, (C) 0.10CoSi, (D) 0.15CoSi, (E) 0.25CoSi, (F) 0.50CoSi

The presence of tricobalt tetroxide was further confirmed by XRD (Fig. 4). Diffraction peaks at 31.3, 36.9, 44.9, 55.7, 59.5 and 65.4 °2θ, corresponding to the crystal planes (220), (311), (400), (422), (511) and (440), respectively, were assigned to face-centred cubic spinel tricobalt tetroxide (JCPDS 42-1467).[34] The cobalt silica xerogel samples were typically amorphous, characterized by a broad peak at ~22 °2θ attributed to the silica matrix.[28] As shown by the inset in Fig. 4, a close examination of the (311) reflection over the 32–43 °2θ region indicated that nanocrystalline Co_3O_4 (<10 nm) was present in the 0.25CoSi and 0.50CoSi xerogels but not in the 0.10CoSi sample. However, the greater intensity of the (311) reflection in 0.50CoSi showed that the concentration of Co_3O_4 was significantly higher than that of 0.25CoSi, which is in good agreement with the spectroscopic results shown previously.

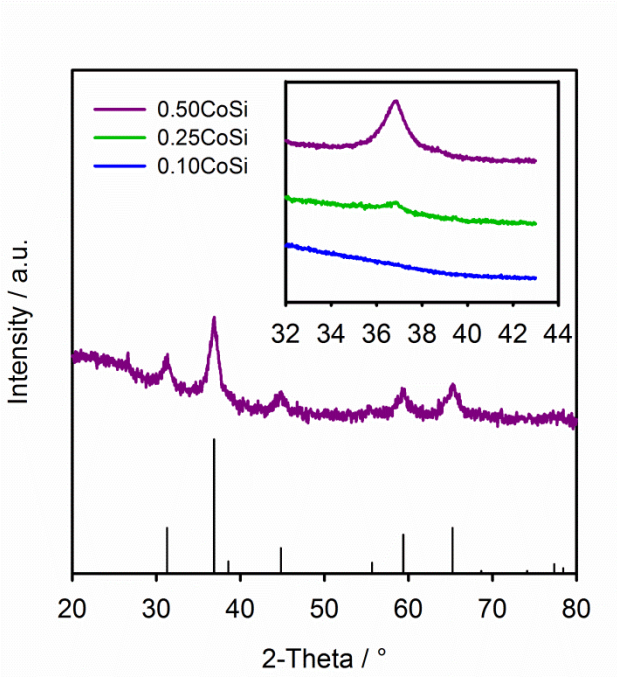

Figure 4: XRD patterns of as-synthesized xerogels and long-time accumulation scans between 32 and 44 °2θ region in the inset.

N_2 sorption was carried out to investigate the effect of cobalt loading on the surface properties and porosity of the bulk xerogels; important characteristics for understanding of the membrane material's molecular sieving microstructure. Figure 5 shows the N_2 sorption isotherms (Fig. 5(a)), BET surface areas (SA) and pore volumes (Fig. 5(b)) for the xerogels. The isotherm for 0.00CoSi was indicative of a dense material with negligible surface area and pore volume. Notably, it was observed that the N_2 sorption isotherms of all the cobalt-incorporated silica xerogels, except the 0.50CoSi sample, exhibited typical Type I profiles with very strong initial adsorption at low partial pressures ($P/P_o < 0.3$) followed by saturation; characteristic of microporous materials. When the Co/Si molar ratio reached 0.50, the sample displayed both microporous-mesoporous texture: adsorption saturation was achieved above 0.7 P/P_o following the multilayer adsorption, with the capillary condensation leading to a small hysteresis loop at 0.5 P/P_o in the desorption stage. All of the cobalt-incorporated silica xerogels had similar specific surface areas of ~240 $m^2\ g^{-1}$ and total pore volumes of ~0.12 $cm^3\ g^{-1}$ without any appreciable differences. The average pore size diameter for 0.05 to 0.25CoSi samples was calculated at ~1.7 nm whilst the 0.50CoSi sample gave a mesoporous structure at ~ 2.5 nm. The average pore size variation was not significant after hydrothermal treatment, though the total pore volume decreased. This densification process was therefore attributed to the loss of micropore volume. Clearly, the incorporation of cobalt significantly

increased the surface area accessible to N_2 compared to the pure silica, similar the results observed elsewhere.[35, 36]

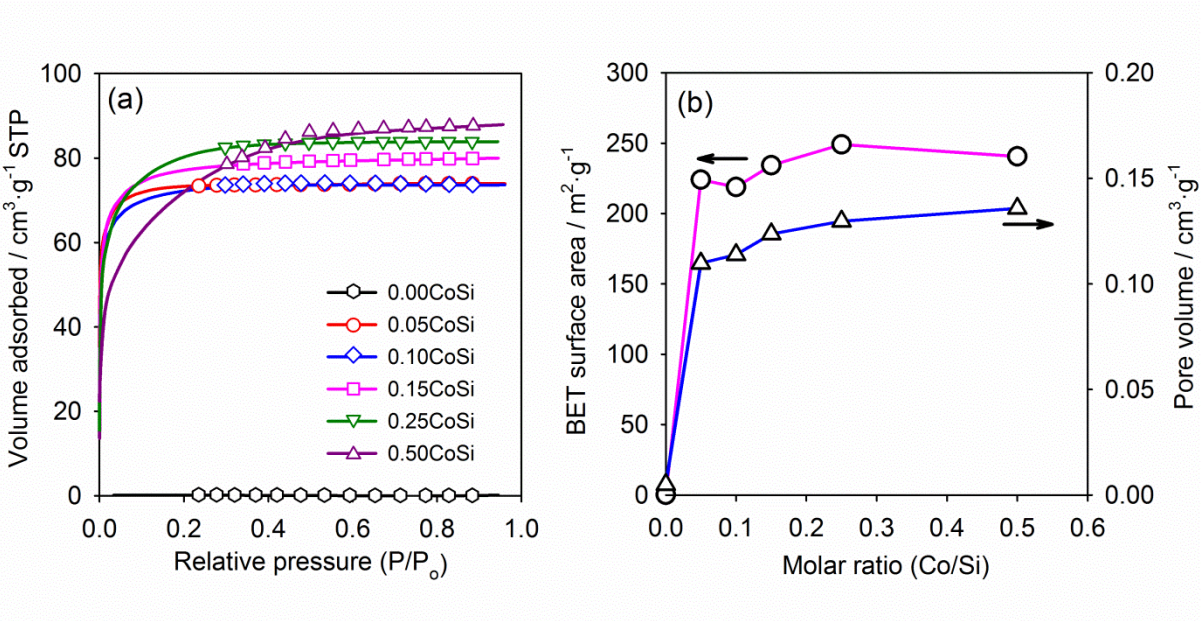

Figure 5: (a) N_2 adsorption (solid line) and desorption (open symbols) isotherms and (b) BET surface area (circle) and pore volume (triangle) of the as-synthesized xerogels (lines are provided as a guide only)

As the molar ratio of Co/Si was increased from 0.10 to 0.25, a dramatic change in the material's morphology was observed by high-resolution transmission electron microscopy (HR-TEM) as shown in Fig. 6. Whilst no cobalt species were detected spectroscopically or by diffraction in 0.10CoSi, the micrograph presented in Fig. 6(a) indicates small clusters of nanoparticles (<5 nm) distributed through the silica network. The larger nuclei of cobalt reduces the transmission of the beam compared to the silicon atom producing a darker shading in the micrograph signifying that these nanoparticles are comprised of a cobalt component. Upon increasing the Co/Si molar ratio to 0.25, large hexagonal-shaped crystals ca. 20 nm in width were observed (Fig. 6(b)), commensurate with the detection of nanocrystalline Co_3O_4 during characterisation. As seen by the small area electron diffractogram (SAED) inset in Fig. 6(b), these particles were crystalline, with interplanar distances of 0.46 nm (111) and 0.24 nm (311) which agree with existing literature (JCPDS 42-1467). [37, 38]

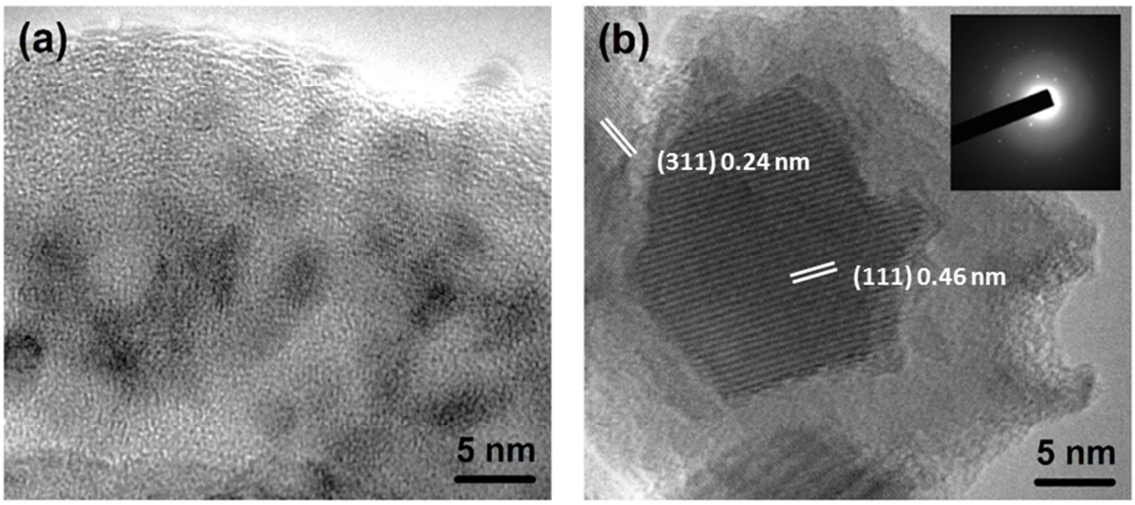

Figure 6: HR-TEM micrographs of (a) 0.10CoSi and (b) 0.25CoSi as-synthesised xerogels with an SAED of the corresponding particles (inset)

3.2 As-synthesized xerogels after hydrothermal treatment

Figure 7 presents the change in surface area of the xerogels after hydrothermal treatment as a function of water vapour content from 10 to 75 mol% at 550 °C for a fixed exposure time of 20 h. The specific surface areas of all samples were observed to be reduced after hydrothermal treatment. It can clearly be seen that the surface area loss was strongly dependent on the Co/Si molar ratio and water vapour content. Firstly, xerogels with Co/Si molar ratio less than 0.25 were found to be extremely unstable, as reflected in the isotherm profiles (Supplementary Information Fig. S2). However, a much more hydrothermally stable structure was observed in 0.25CoSi and 0.50CoSi. The latter only produced small surface area losses of 7.4 and 10.5 % after 25 and 75 mol% water vapour treatments, respectively. The isotherm profiles of these treated samples were found to be indifferent to that of their as-synthesized counterparts, thus confirming that hydrothermal treatment had not negatively impacted on the material's microstructure. From this investigation, it can be concluded that the vapour content had only a small effect on the high cobalt-incorporated samples (0.25CoSi and 0.50CoSi) despite their chemical constituents containing a significantly higher concentration of surface silanol groups.

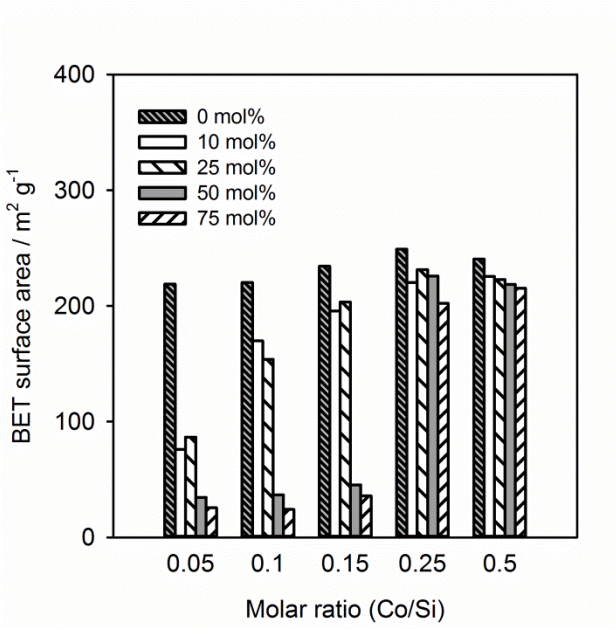

Figure 7: BET Surface area of the xerogels as a function of Co/Si molar ratio and vapour content at 550 °C and 20 h.

Further examinations into the temporal effect and water vapour concentration were also performed. Fig. 8 shows the surface area loss of the xerogels after being subjected to 25 or 75 mol% vapour for different exposure durations. The effect of exposure time had a significant impact on the structural stability of xerogels, particularly in samples with low cobalt loadings (Co/Si< 0.25) in the 25 mol% vapour condition. In Fig. 8(a), the greatest loss in surface area can be observed for 0.15CoSi. This sample appeared to be quite stable after 20 h treatment with only a surface area loss of 13 %, but suffered an 80 % loss after 100 h of treatment. Under the same treatment conditions, a greater surface area loss was induced after 20 h for 0.05CoSi and 0.10CoSi, reaching a maximum of ca. 85 % after 100 h treatment. These results indicate that 0.05CoSi and 0.10CoSi were more susceptible to hydrothermal densification, especially when compared to 0.25CoSi and 0.50CoSi which both reported less than 15 % surface area loss after 100 h.

The effect of vapour content was more enhanced for the 75 mol% water vapour treatment as shown in Fig. 8(b). A similar trend can be observed in this investigation whereby cobalt concentration again played a major role. It is interesting to point out that the surface area loss of all of the xerogels after 20 h treatment was mirrored by the results from the 100 h treatment in 25 mol% vapour. This is not surprising as this treatment condition is considered to be extremely harsh, and meets the expectation of the maximum industrial condition for wet gas separation. Under this treatment condition, only 0.25CoSi and 0.50CoSi exhibited a

minimal degree of hydrothermal densification even after 40 h treatment, which was detrimental for 0.05CoSi, 0.10CoSi and 0.15CoSi. In contrast, the incremental losses of the samples' surface area between 20 and 40 h treatment in the 75 mol% vapour condition (Fig. 8(b)) were only found to be between 5–10 % for all samples. This could be explained by an equilibrium state establishing after the xerogels saturate with vapour causing rapid densification within 20 h exposure, whereby only marginal densification occurs with further temporal exposure.

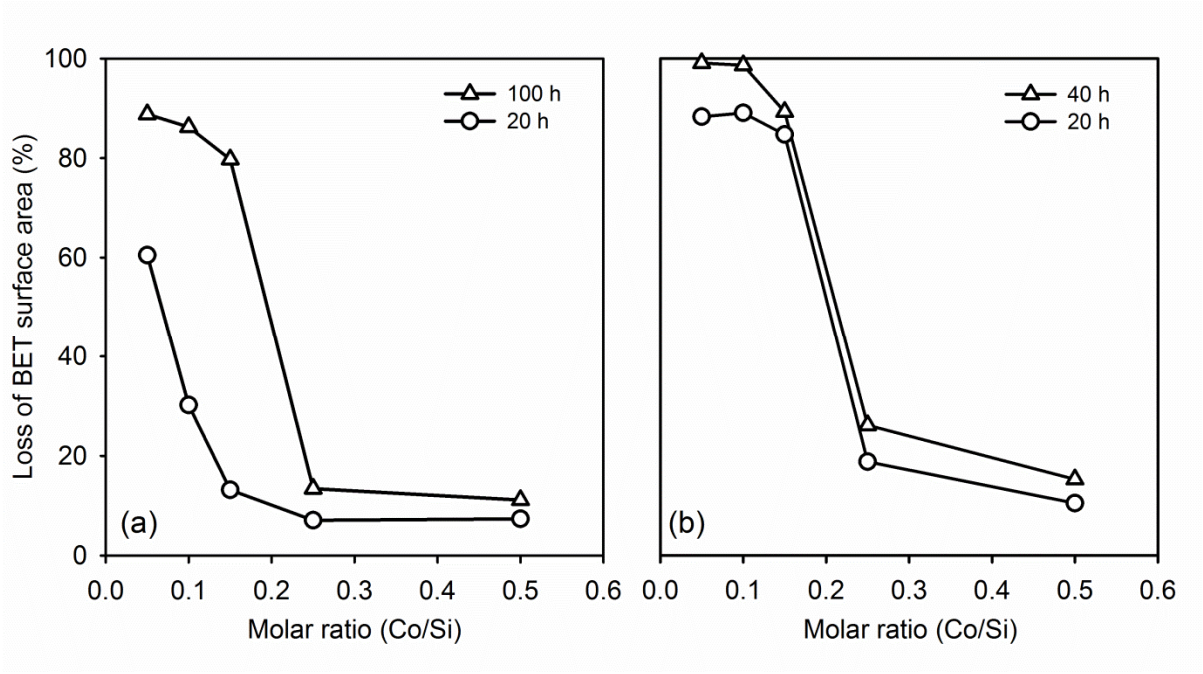

Figure 8: Surface area loss of the xerogels for the (a) 25 and (b) 75 mol% vapour content as a function of Co/Si molar ratio and exposure time at 550 °C (lines are provided as a guide only)

As shown in Fig. 9, the effect of temperature on the xerogels at constant water vapour condition and exposure time (250, 350, and 550 °C; 75 mol% vapour; 20 h) trended similarly to those of previously discussed treatment conditions. Irrespective of treatment temperature the densification was most severe in samples with relatively low cobalt loading when treated with 75 mol% water vapour, whilst only marginal differences were observed for 0.25CoSi and 0.50CoSi. These results suggest that the effect of hydrothermal treatment on the xerogels investigated in this study was not strongly dependent on the exposure time (Fig. 8(b)) or temperature (Fig. 9) under such high vapour conditions (75 mol%).

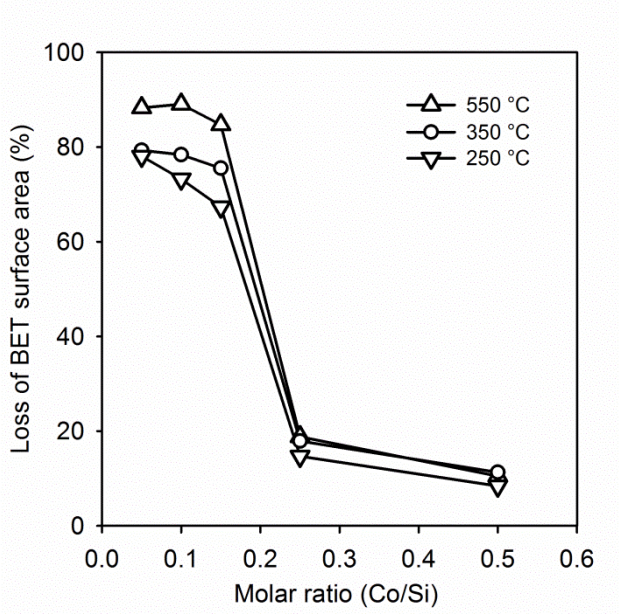

Figure 9: Surface area loss of xerogels as a function of Co/Si molar ratio and temperature at 75 mol% vapour and 20 h (lines are provided as a guide only).

The FTIR spectra of the treated xerogels exposed to 550 °C, 75 mol% vapour and 40 h are shown in Fig. 10. All spectra exhibited characteristic vibrational modes of siloxane and silanol groups typical of a silica network. Interestingly, it can be observed that the peak maxima position of the Si–O–Si TO vibrational mode of all treated samples was detected at the same frequency, ~1045 cm^{-1}. In comparison, the change in the frequency of this band for the treated samples was only observed for the low cobalt incorporated xerogels (0.05CoSi, 0.10CoSi and 0.15CoSi) whereas the position of this band was unaffected for 0.25CoSi and 0.50CoSi. Similarly, the peak intensity of the silanol groups (950 cm^{-1}) for 0.25CoSi and 0.50CoSi was higher than that of 0.05CoSi, 0.10CoSi and 0.15CoSi, although the change between pre- and post-treatment was neglible in each case. The presence of tricobalt tetroxide (~670 cm^{-1}) was again only observed in 0.25CoSi and 0.50CoSi suggesting that Co_3O_4 remained as a stable phase during the hydrothermal treatment. This was also confirmed by the Raman spectra of the corresponding treated xerogels (Supplementary Information Fig. S3).

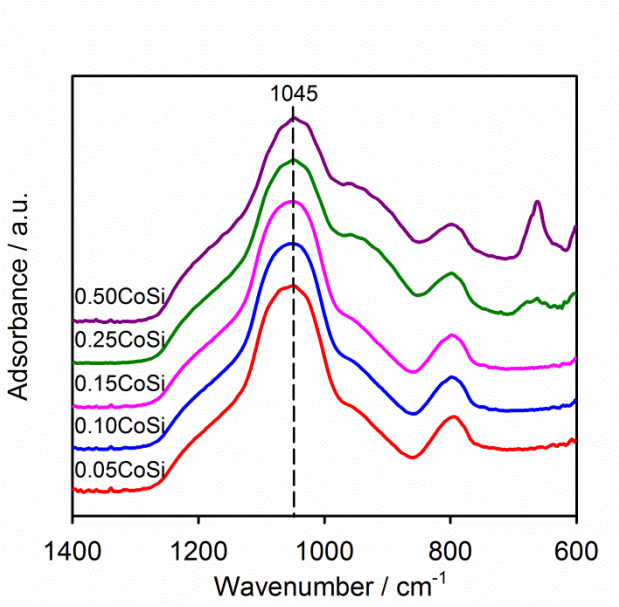

Figure 10: FTIR spectra of the xerogels exposed to 550 °C, 75 mol% vapour and 40 h.

To further probe the silica structure evolution, the treated xerogel powders of 0.10CoSi (unstable) and 0.25CoSi (stable) were analysed by ^{29}Si CP/MAS NMR (Supplementary Information Fig. S4). The percentage variation of Q^n species populations of the treated xerogels compared with the as-synthesised xerogels is shown in Fig. 11. This variation was determined from the area difference of the decomposed peaks associated with each Q^n species before and after hydrothermal treatment. A large increase of the Q^4 group was observed for the 0.10CoSi sample after treatment indicating further condensation took place during treatment. This conjecture is clearly supported by the loss in both the Q^2 and Q^3 groups whereby the silanol groups underwent crosslinking to form the fully condensed siloxane species. On the other hand, only a minor change in the Q^n species was observed for 0.25CoSi, albeit with a small decrease in the Q^2 group which had predominately converted to the Q^3 specie. This suggests that the structural rearrangement of the silanol and siloxane groups was minimal; hence the material was more stable. These findings are in good agreement with the hydrothermal results of the xerogels via N_2 sorption.

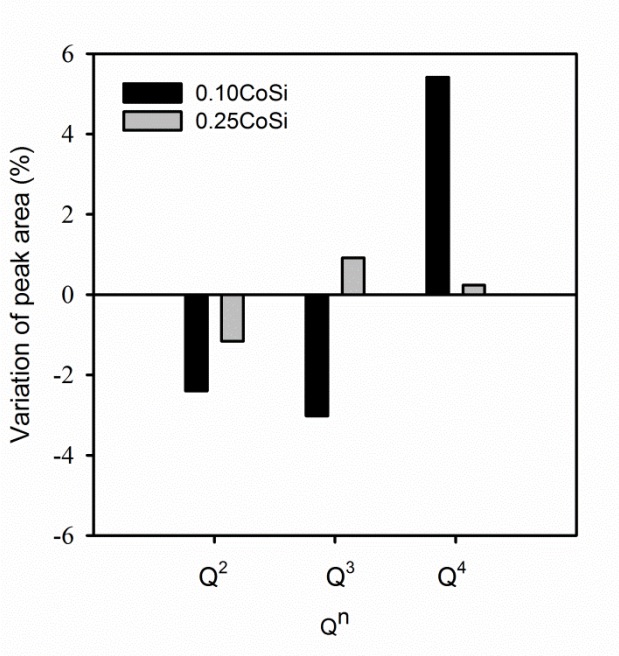

Figure 11: Percentage variation of decomposed peak area of the silicon Q^n species between the as-synthesised and the treated xerogel samples (0.10 CoSi and 0.25CoSi)

3.3 Discussion

From the hydrothermal investigations of the as-synthesised CoSi xerogels, it was clearly discerned that both 0.25CoSi and 0.50CoSi outperformed the xerogels with lower cobalt-incorporation over all testing conditions. It is widely accepted that the instability of silica is due to the hydrolytic attack by water molecules leading to restructuring of the silica matrices. [10] This conjecture is often pitched by the degree of hydrophilicity associated with the silanol groups on the surface in the literature; the more hydrophilic silanol groups on the surface the greater the susceptibility to hydrolysis. Nevertheless, the silanol groups are important for the pore size tailoring of the silica network in creating a molecular sieving pore structure. In this xerogel investigation, it was noteworthy that the hydrothermally stable xerogels (0.25CoSi and 0.50CoSi) had a relatively high silanol ratio as determined from the FTIR and ^{29}Si CP/MAS NMR results. Meanwhile, xerogels with a lower silanol ratio were not observed to produce a hydrothermally stable structure. Therefore, the hydrothermal stability cannot strictly be related to the silanol ratio in this case.

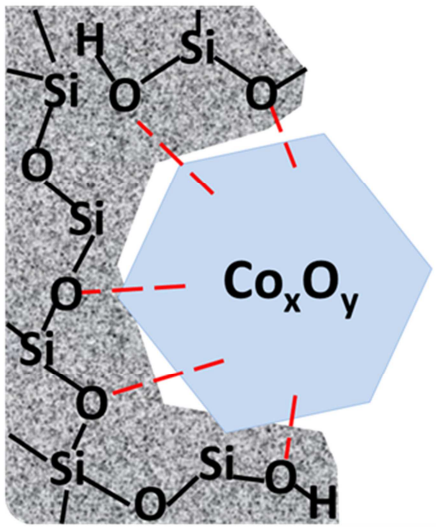

Figure 12: Scheme of the interaction between cobalt oxide (Co_xO_y) and silica network.

It was interesting to observe a correlation that xerogels with low cobalt concentrations (0.05CoSi, 0.10CoSi and 0.15CoSi) had undetectable cobalt species and concurrently demonstrated hydrothermally unstable matrices. These results strongly implicate that Co_3O_4 was a responsible factor in maintaining the structural stability of the matrices in this work, as suggested by its stabilising influence on membranes tested under mild hydrothermal conditions.[11, 18, 21, 22] Despite of all these studies, the mechanism behind this experimental observation is still not well understood or explained.

It is believed that a strong physical bonding interaction between the cobalt oxides and the silica matrix is responsible for the improved hydrothermal stability. As depicted in Fig. 12, the bonding interaction between the cobalt oxide species (Co_xO_y) and the oxygen atoms of the silanol groups and siloxane bridges is only possible where these groups are in close proximity in the matrix. Indeed, when more cobalt was incorporated, a higher concentration of Co_xO_y is expected inside the silica matrix; especially Co_3O_4 which correlated with the improved hydrothermal stability in this study. This interaction was most evident in the FTIR results (Fig. 2(a)) where a significant redshift in the asymmetric Si–O–Si stretching vibration was observed with increasing cobalt concentration. Similar behaviour has also been reported by Parler et al.[30] and Clapsaddle et al.[39] for cobalt oxide silica and iron oxide silica systems, respectively. This behaviour has been hypothesized to relate to a reduction in the bond strength of the Si–O–Si vibration as a result of a change in the dipole moments of the siloxane bridges.[30] However, an increasing interaction between the Co_xO_y and the silica must

play an important role in preventing the siloxane bridges from hydrolytic attack by water molecules even at extremely harsh hydrothermal condition (550 °C, 75 mol%, 40 h).

To further understand the mechanism behind hydrothermal stability, a structural model is proposed as shown in Fig. 13. Due to the low concentration of Co_xO_y in the 0.05, 0.10 and 0.15CoSi samples (Fig. 6(a)), a smaller degree of physical interaction with the silica surface would be expected. In addition, the small degree of this interaction would barely be detected by the change in the siloxane bridge vibration as indicated in Fig. 2(a). Hence, the internal silica surface (i.e. surface of the micropores) exposed to water molecules during hydrothermal treatment would be much greater and more susceptible to hydrolysis, leading to further condensation and densification. As such, the xerogels lose a considerable proportion of their initial surface area and pore volume (> 90 % maximum reduction). This is supported by the ^{29}Si CP/MAS NMR study presented in Fig. 11 and the hydrothermal results. In other words, the densification leading to pore shrinkage of the silica matrix must have brought them closer within the pores. Therefore, an increased physical interaction between Co_xO_y and the silica is expected and was observed in the FTIR spectra (Fig. 10) by a redshift in the siloxane bridge vibrations to ~1045 cm^{-1} for 0.05CoSi, 0.10CoSi and 0.15CoSi. This constitutes a significant shift of 44 cm^{-1} wavenumbers.

Meanwhile, when the cobalt concentration reached a critical threshold (Co/Si $\geq$ 0.25), crystalline Co_3O_4 particles were clearly detected (Fig. 4 and 6(b)). For these samples, 0.25CoSi and 0.50CoSi, the presence of Co_3O_4 in the silica matrices and their strong physical interaction with the silica matrix provided superior hydrothermal stability. As shown schematically in Fig. 13, this interaction was envisaged to be much stronger and long range due to the large particle size of crystalline Co_3O_4 and possibly also other forms of untraceable Co_xO_y. Despite a smaller degree of densification observed (SA and PV < 25 % maximum reduction), the majority of the silica matrix in physical interaction with the Co_3O_4 was "shielded" from hydrolysis. Therefore, only a small concentration of Q^2 groups was condensed in forming the Q^3 species after the hydrothermal treatment and that structural integrity was maintained throughout the various hydrothermal exposure conditions.

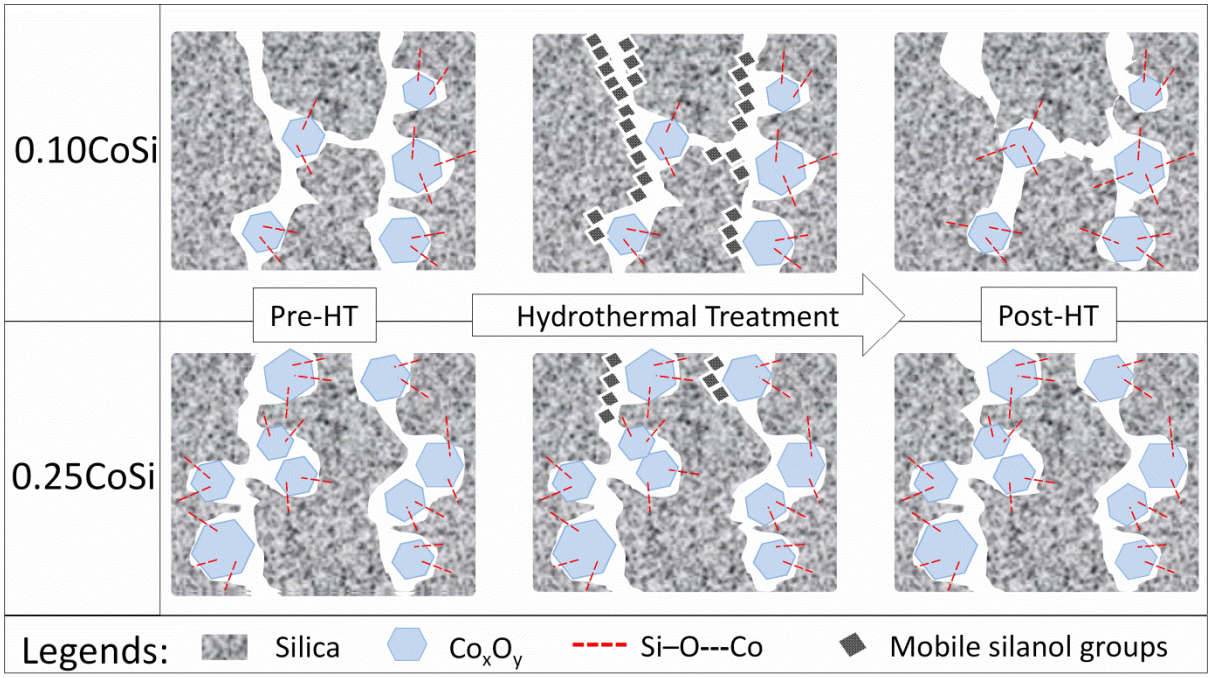

Figure 13: Proposed model for the structural and textural evolution of 0.10CoSi (unstable) and the 0.25CoSi (stable) xerogel samples pre and post hydrothermal treatment.

Conclusions:

Cobalt silica xerogels were synthesized via sol-gel processing, incorporating a systematic increase of Co/Si molar ratio (0.00-0.50). The degree of condensation of the silica network and the formation of tricobalt tetroxide (Co_3O_4) were governed by the cobalt-loading. High cobalt-loading samples (0.25CoSi and 0.50CoSi) produced greater concentrations of silanol groups and nanocrystalline Co_3O_4 as evidenced by FTIR, ^{29}Si CP/MAS NMR, micro-Raman and XRD. Co_3O_4 was the only detected crystalline phase in the silica matrix and it was not observed in the xerogels with a low cobalt-loading (0.05CoSi, 0.10CoSi and 0.15CoSi).

The results of hydrothermal investigation revealed that 0.05CoSi, 0.10CoSi and 0.15CoSi were susceptible to the treatment conditions while 0.25CoSi and 0.50CoSi maintained their structural integrity under a full range of treatment conditions. Furthermore, it was shown that the hydrothermal stability of the xerogels was not directly associated with the concentration of hydrophilic silanol groups. Meanwhile, the materials' stability correlated well with the presence of Co_3O_4 in 0.25CoSi and 0.50CoSi. A structural model was proposed which explained that the interaction between Co_xO_y particles and the silica matrix confers improved hydrothermal stability.

Acknowledgements:

Liang Liu would like to acknowledge the scholarship from The University of Queensland and CO2CRC - Cooperative Research Centre for Greenhouse Gas Technologies. The authors would like to acknowledge financial support provided by the Australian Government through its CRC program to support this CO2CRC research project. The authors acknowledge the facilities, and the scientific and technical assistance, of the Australian Microscopy & Microanalysis Research Facility at the Centre for Microscopy and Microanalysis, The University of Queensland. Raman spectroscopy was performed at the Bio-Nano Development Facility in the Australian Institute for Bioengineering and Nanotechnology, which was funded by the Queensland State Government Smart State Innovation Building Fund. David Wang acknowledges funding support from the Australian Research Council (DP110101185).

References

1. C. G. Guizard, A. C. Julbe and A. Ayral, *J. Mater. Chem.*, 1999, **9**, 55-65.
2. M. S. P. Francisco and Y. Gushikem, *J. Mater. Chem.*, 2002, **12**, 2552-2558.
3. A. Martucci, D. Buso, M. D. Monte, M. Guglielmi, C. Cantalini and C. Sada, *J. Mater. Chem.*, 2004, **14**, 2889-2895.
4. G. Olguin, C. Yacou, S. Smart and J. C. Diniz da Costa, *Sci. Rep.*, 2013, **3**, No. 2449.
5. C. Yacou, M.-L. Fontaine, A. Ayral, P. Lacroix-Desmazes, P.-A. Albouy and A. Julbe, *J. Mater. Chem.*, 2008, **18**, 4274-4279.
6. R. M. de Vos and H. Verweij, *Science*, 1998, **279**, 1710-1711.
7. C. Y. Tsai, S. Y. Tam, Y. Lu and C. J. Brinker, *J. Membr. Sci.*, 2000, **169**, 255-268.
8. Y. Lin, I. Kumakiri, B. Nair and H. Alsyouri, *Sep. Purif. Rev.*, 2002, **31**, 229-379.
9. T. A. Witten and M. Cates, *Science*, 1986, **232**, 1607-1612.
10. M. C. Duke, J. C. Diniz da Costa, D. D. Do, P. G. Gray and G. Q. Lu, *Adv. Funct. Mater.*, 2006, **16**, 1215-1220.
11. C. X. C. Lin, L. P. Ding, S. Smart and J. C. Diniz da Costa, *J. Colloid Interface Sci.*, 2012, **368**, 70-76.
12. Y. F. Gu, P. Hacarlioglu and S. T. Oyama, *J. Membr. Sci.*, 2008, **310**, 28-37.
13. T. Tsuru, K. Yamaguchi, T. Yoshioka and M. Asaeda, *AIChE J.*, 2004, **50**, 2794-2805.
14. R. M. De Vos, W. F. Maier and H. Verweij, *J. Membr. Sci.*, 1999, **158**, 277-288.
15. H. L. Castricum, A. Sah, M. C. Mittelmeijer-Hazeleger, C. Huiskes and J. E. t. Elshof, *J. Mater. Chem.*, 2007, **17**, 1509-1517.
16. M. C. Duke, J. C. Diniz da Costa, G. Q. Lu, M. Petch and P. Gray, *J. Membr. Sci.*, 2004, **241**, 325-333.
17. M. Kanezashi and M. Asaeda, *J. Membr. Sci.*, 2006, **271**, 86-93.
18. R. Igi, T. Yoshioka, Y. H. Ikuhara, Y. Iwamoto and T. Tsuru, *J. Am. Ceram. Soc.*, 2008, **91**, 2975-2981.
19. D. Uhlmann, S. Liu, B. P. Ladewig and J. C. Diniz da Costa, *J. Membr. Sci.*, 2009, **326**, 316-321.
20. V. Boffa, D. H. A. Blank and J. E. t. Elshof, *J. Membr. Sci.*, 2008, **319**, 256-263.
21. D. Uhlmann, S. Smart and J. C. Diniz da Costa, *Sep. Purif. Technol.*, 2010, **76**, 171-178.
22. S. Battersby, S. Smart, B. Ladewig, S. Liu, M. C. Duke, V. Rudolph and J. C. Diniz da Costa, *Sep. Purif. Technol.*, 2009, **66**, 299-305.

23. C. J. Brinker and G. W. Scherer, *Sol-gel science: the physics and chemistry of sol-gel processing*, Academic Pr, 1990.
24. Z. Olejniczak, M. Łęczka, K. Cholewa-Kowalska, K. Wojtach, M. Rokita and W. Mozgawa, *J. Mol. Struct.*, 2005, **744**, 465-471.
25. D. M. Pickup, G. Mountjoy, M. A. Holland, G. W. Wallidge, R. J. Newport and M. E. Smith, *J. Mater. Chem.*, 2000, **10**, 1887-1894.
26. P. Innocenzi, *J. Non-Cryst. Solids*, 2003, **316**, 309-319.
27. A. Bertoluzza, C. Fagnano, M. Antonietta Morelli, V. Gottardi and M. Guglielmi, *J. Non-Cryst. Solids*, 1982, **48**, 117-128.
28. G. Ortega-Zarzosa, C. Araujo-Andrade, M. Compeán-Jasso, J. Martínez and F. Ruiz, *J. Sol-Gel Sci. Technol.*, 2002, **24**, 23-29.
29. S. Esposito, M. Turco, G. Ramis, G. Bagnasco, P. Pernice, C. Pagliuca, M. Bevilacqua and A. Aronne, *J. Solid State Chem.*, 2007, **180**, 3341-3350.
30. C. M. Parler, J. A. Ritter and M. D. Amiridis, *J. Non-Cryst. Solids*, 2001, **279**, 119-125.
31. C. Brinker, R. Kirkpatrick, D. Tallant, B. Bunker and B. Montez, *J. Non-Cryst. Solids*, 1988, **99**, 418-428.
32. V. Hadjiev, M. Iliev and I. Vergilov, *Journal of Physics C: Solid State Physics*, 1988, **21**, L199.
33. C. R. Miller, D. K. Wang, S. Smart and J. C. Diniz da Costa, *Sci. Rep.*, 2013, **3**, No. 1648.
34. G. A. Santos, C. Santos, S. W. da Silva, E. A. Urquieta-González and P. P. C. Sartoratto, *Colloids Surf., A*, 2012, **395**, 217-224.
35. S. Smart, J. F. Vente and J. C. Diniz da Costa, *Int. J. Hydrogen Energy*, 2012, **37**, 12700-12707.
36. C. Yacou, S. Smart and J. C. Diniz da Costa, *Energy Environ Sci.*, 2012, **5**, 5820-5832.
37. J. Liu, H. Xia, L. Lu and D. Xue, *J. Mater. Chem.*, 2010, **20**, 1506-1510.
38. Y. Liu, G. Zhu, B. Ge, H. Zhou, A. Yuan and X. Shen, *CrystEngComm*, 2012, **14**, 6264-6270.
39. B. J. Clapsaddle, A. E. Gash, J. H. Satcher Jr and R. L. Simpson, *J. Non-Cryst. Solids*, 2003, **331**, 190-201.